# Multi-Satellite Altimeter Validation along the French Atlantic Coast in the Southern Bay of Biscay from ERS-2 to SARAL

**Phuong Lan Vu [1],\*** [ID]**, Frédéric Frappart [1,2], José Darrozes [1], Vincent Marieu [3], Fabien Blarel [2], Guillaume Ramillien [1], Pascal Bonnefond [4] and Florence Birol [2]**

[1]   GET-GRGS, UMR 5563, CNRS/IRD/UPS, Observatoire Midi-Pyrénées, 14 Avenue Edouard Belin, 31400 Toulouse, France; frederic.frappart@get.omp.eu (F.F.); jose.darrozes@get.omp.eu (J.D.); Guillaume.Ramillien@get.omp.eu (G.R.)

[2]   LEGOS-GRGS, UMR 5566, CNES/CNRS/IRD/UPS, Observatoire Midi-Pyrénées, 14 Avenue Edouard Belin, 31400 Toulouse, France; florence.birol@legos.obs-mip.fr (F.B.); fabien.blarel@legos.obs-mip.fr (F.B.)

[3]   UMR CNRS 5805 EPOC—OASU—Université de Bordeaux, Allée Geoffroy Saint-Hilaire CS 50023, 33615 Pessac CEDEX, France; vincent.marieu@u-bordeaux.fr

[4]   SYRTE, Observatoire de Paris, PSL Research University, CNRS, Sorbonne Universités, UPMC Univ. Paris 06, LNE, 75014 Paris, France; pascal.bonnefond@obspm.fr

\*   Correspondence: phuonglan.vu@get.omp.eu; Tel.: +33-7-8232-1136

**Abstract:** Monitoring changes in coastal sea levels is necessary given the impacts of climate change. Information on the sea level and its changes are important parameters in connection to climate change processes. In this study, radar altimetry data from successive satellite missions, European Remote Sensing-2 (ERS-2), Jason-1, Envisat, Jason-2, and Satellite with ARgos and ALtiKa (SARAL), were used to measure sea surface heights (SSH). Altimetry-derived SSH was validated for the southern Bay of Biscay, using records from seven tide gauges located along the French Atlantic coast. More detailed comparisons were performed at La Rochelle, as this was the only tide gauge whose records covered the entire observation period for the different radar altimetry missions. The results of the comparison between the altimetry-based and in-situ SSH, recorded from zero to five kilometers away from the coast, had root mean square errors (RMSE) ranging from 0.08 m to 0.21 m, 0.17 m to 0.34 m, 0.1 m to 0.29 m, 0.18 m to 0.9 m, and 0.22 m to 0.89 m for SARAL, Jason-2, Jason-1, ENVISAT, and ERS-2, respectively. Comparing the missions on the same orbit, ENVISAT had better results than ERS-2, which can be accounted for by the improvements in the sensor mode of operation, whereas the better results obtained using SARAL are related to the first-time use of the Ka-band for an altimetry sensor. For Jason-1 and Jason-2, improvements were found in the ocean retracking algorithm (MLE-4 against MLE-3), and also in the bi-frequency ionosphere and radiometer wet troposphere corrections. Close to the shore, the use of model-based ionosphere (GIM) and wet troposphere (ECMWF) corrections, as applied to land surfaces, reduced the error on the SSH estimates.

**Keywords:** sea surface height; coastal altimetry; validation; tide gauge

## 1. Introduction

Satellite altimetry is a radar technique detailing the topography of the earth's surface based on the measurement of the distance between the satellite and the surface, derived from the two-way travel time of an electromagnetic wave emitted by the altimeter, or altimeter range and the precise knowledge of the satellite orbit [1,2]. The primary objectives of satellite radar altimetry are to measure the marine geoid, ocean currents, and sea level variability. In the coastal zones, sea level data retrieval and interpretation is particularly complex. This is due to the interaction of the radar signal with

land topography [3–6], geophysical corrections becoming inaccurate or incorrect when land surfaces are encompassed by the footprint of altimeters and radiometers [7], and to the short time scales and small spatial scales of the coastal dynamics [8] that are only partly sampled by the different altimeter missions, even when used in conjunction. Advances were made in altimeter instrument design with the development and launch of the Ka-band AltiKa instrument with on-board Satellite with ARgos and ALtiKa (SARAL). The use of this higher frequency reduces noise and has a smaller radar footprint in the images than in those obtained with the classical Ku-band instruments [9]. As a result, the coastal band is reduced where echoes are impacted by the presence of land. The launches of the first altimeters using the Synthetic Aperture Radar (SAR) technique [10], SIRAL on-board Cryosat-2 and SRAL on-board Sentinel-3, allowed more reliable observations in coastal areas. In parallel, advances were made in the development of new processing algorithms, corrections, and products for coastal applications of radar altimetry [11–14].

In this study, a comparison was completed of the most-used altimetry missions for monitoring the dynamic topography of the ocean surface, Jason-1, Jason-2, ERS-2, Envisat, and SARAL on their nominal tracks, operating in Low Resolution Mode (LRM) along the Atlantic coast of the Bay of Biscay (42–48°N, 0–10°W) from 1993 to 2015. Compared to the permanent calibration facilities or Calibration/Validation (Cal/Val) sites, parts of the ESA Earth Observation ground segment are located in Corsica, the Western Mediterranean Sea at the Harvest platform [15], the Eastern Pacific Ocean in Gavdos [16], the Eastern Mediterranean Sea [17], and the Bass Strait, between Australia and Tasmania [18]. Our goal was to evaluate the quality of altimeter-based sea surface heights (SSH). Our study had two main interests: to be well-instrumented with the presence of seven tide gauges in close proximity to eight altimeter tracks from five altimetry missions (Figure 1), and to investigate different tidal conditions than the classical altimetry Cal/Val sites. In contrast to the Corsica and Gavdos Mediterranean sites that are in semi-diurnal micro-tidal environments, the Harvest platform on the Pacific coast of California and the Bass Strait site between Australia and Tasmania are in mixed semi-diurnal macro and micro-tidal environments, respectively. The Bay of Biscay study area is in a semi-diurnal macro-tidal environment [19–21].

The error in the SSH retrieval from radar altimetry is caused by two main components: the ionosphere and wet troposphere corrections. For all satellites, the Ionosphere Correction (IC), due to electron content in the ionosphere, is obtained either by the bi-frequency altimeters, in Ku and C bands for T/P, Jason-1/2, and in Ku and S bands for Envisat, or from the electronic content of the ionosphere, such as the Global Ionospheric Maps (GIM) [22], available after 1998, or the New Ionospheric Climatology 2009 (NIC 09) [23] for mono-frequency altimeters such as ERS-2 or SARAL. The Wet Troposphere Correction (WTC), due to liquid water in the atmosphere, is derived either from radiometer measurements present on altimetry satellites or from meteorological model outputs, such as the ones made available by the European Center for Medium Range Weather Forecasting (ECMWF). Bi-frequency and radiometer-based corrections are used over the ocean even in coastal areas.

This study assessed the altimetry-based SSH in terms of number of observations, bias, root mean square error (RMSE), and correlation coefficient, for almost all the missions that were in orbit between 1993 and 2015, using records from seven tide gauges located along the French Atlantic coast in the southern Bay of Biscay. Contrary to what is commonly performed when using radar altimetry in coastal areas, the performance was assessed for different combinations of corrections applied to the altimeter range available in the Geophysical Data Records (GDR). A detailed analysis of the impact of these corrections on the accuracy of the altimetry-based SSH was performed at the La Rochelle tide gauge because this tide gauge is the only one that covers the entire observation period for the different radar altimetry missions.

## 2. Datasets and Study Area

### 2.1. Radar Altimetry Data

The radar altimetry data used in this study was obtained from the high precision altimetry missions launched after 1992 with the exception of Topex/Poseidon and Geosat Follow-On. Figure 1 shows a timeline of the different missions. The data were made available by the Centre de Topographie de l'Océan et de l'Hydrosphère (CTOH [24]). Altimetry data from all satellites were corrected for the classical propagation and geophysical corrections needed from the coast, including instrumental, ionosphere, wet and dry troposphere, sea state bias, solid earth, and pole tide corrections.
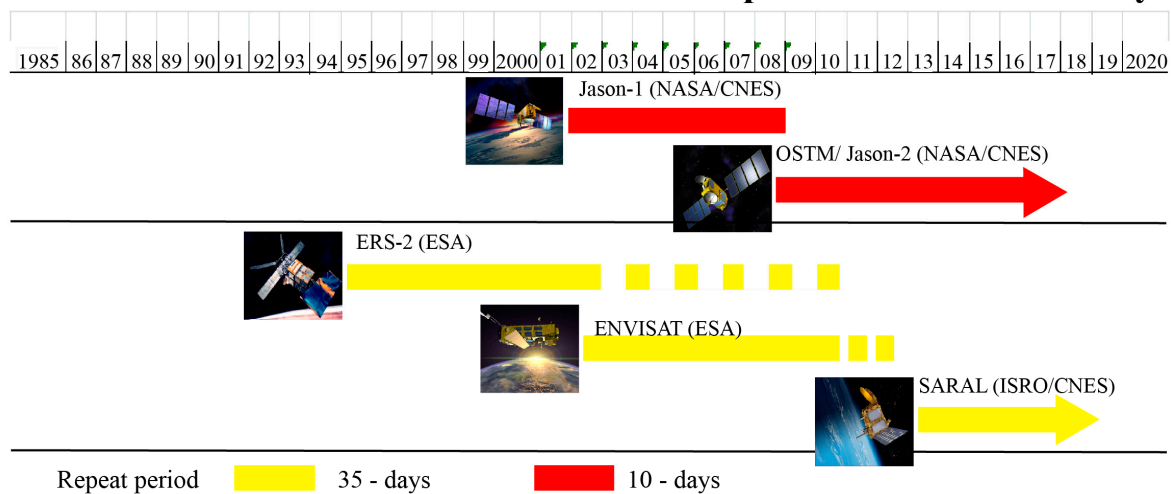


**Figure 1.** Timeline for radar altimeters used in our study (modified from [25]).

### 2.1.1. Jason-1

This mission was launched in December 2001 by the National Aeronautics and Space Administration (NASA) and the Centre national d'études spatiales (CNES) to ensure continuity of the oceanographic observations provided by the Topex/Poseidon mission. The Jason-1 payload is composed of the Poseidon-2 altimeter operating at Ku (13.575 GHz) and C (5.3 GHz) bands, a microwave radiometer, and a triple system for precise orbit determination [26] Jason-1 orbits at an average altitude of 1336 km, with an inclination of 66°, on a 10-day repeating cycle. Observations along the ground track of all ocean and continental surfaces from these altimeters are collected from 66°N to 66°S.

### 2.1.2. Jason-2

The Jason-2 mission was launched on 20 June 2008 as a co-operation between CNES, EUMESAT, NASA, and The National Oceanic and Atmospheric Administration (NOAA). Its payload is mostly composed of the Poseidon-3 radar altimeter from CNES, the Advanced Microwave Radiometer (AMR) from JPL/NASA, and a triple system for precise orbit determination: the real-time tracking system Détermination Immédiate d'Orbite par Doris Embarqué (DIODE) of the Doppler Orbitography by Radiopositioning Integrated on Satellite (DORIS) instrument from CNES, a Global Positioning System (GPS) receiver and a Laser Reflector Array (LRA) from NASA. Jason-1 and Jason-2 share the same orbit of 1336 km above the earth, with a cycle time of 10 days. Poseidon-3 radar altimeter is a two-frequency solid-state altimeter that accurately measures the distance between the satellite and the surface (range). It also provides ionospheric delay corrections over the ocean with a precision of about 2 cm, operating at Ku (13.575 GHz) and C (5.3 GHz) bands [25,27].

### 2.1.3. ERS-2

European Remote Sensing-2 (ERS-2) was launched in 1995 by the European Space Agency (ESA) as an ERS-1 follow-up mission, designed to study the earth's environment. The satellite carries, among other instruments, a radar altimeter (RA) operating at Ku-band (13.8 GHz), developed for measuring the height of the ocean, land, and ice caps. ERS-2 orbits at an average altitude of 790 km, with an inclination of 98.54°, on a sun-synchronous orbit with a 35-day repeating cycle. It provides observations of the earth's surface, including ocean, land, and ice caps, from 82.4°N to 82.4°S. This orbit was formerly used by the ERS-1 mission, with an equatorial ground-track spacing of about 85 km. ERS-2 data are available from 17 May 1995 to 9 August 2010. After 22 June 2003, the dataset coverage is limited to ground station visibility.

### 2.1.4. Envisat

The Envisat mission was launched on 1 March 2002 by ESA, carrying 10 instruments including the advanced radar altimeter (RA-2). Envisat was based on the on-board sensor on the ERS-1 and 2 satellites. RA-2 was a nadir-looking pulse-limited radar altimeter operating at two frequencies at the Ku (13.575 GHz), as ERS-1 and 2, and S (3.2 GHz) bands. The goal was to collect radar altimetry data over ocean, land, and ice caps [26,28] Envisat remained on its nominal orbit until October 2010 and its mission ended 8 April 2012. RA-2 stopped operating correctly at S-band in January 2008. Its initial orbital characteristics were the same as for ERS-2.

### 2.1.5. SARAL/AltiKa

The SARAL mission was launched on 25 February 2013. SARAL is collaboration between CNES and Indian Space Research Organization (ISRO). Its payload included the AltiKa radar altimeter and bi-frequency radiometer, and a triple system for precise orbit determination: the real-time tracking system DIODE of DORIS instrument, a Laser Reflector Array (LRA), and the Advance Research and Global Observation Satellite (ARGOS-3). The AltiKa radar altimeter is a solid-state mono-frequency altimeter that provides accurate range measurements and is the first altimeter to operate Ka-band (35.75 GHz). Formerly, the SARAL orbit was used by ERS-1 and 2 and Envisat, with an equatorial ground-track spacing of about 85 km [9], and a 35-day repeating cycle. It was placed on a drifting orbit as of 7 April 2016.

### 2.2. Tide Gauge Records

The tidal data used in this study was obtained from records of tide gauges SSH from the French Réseaux de référence des observations marégraphiques (REFMAR) networks [29]. We used data from 7 tide gauge stations located along the southwestern coast of France (Table 1; Figure 1). The SSH data were provided at 10-min intervals and were referenced to the Institut Géographique National 1969 (IGN69) ellipsoid. For comparison with the altimetry data, the difference between the two reference systems (ZH/GRS80 in Table 1) was calibrated at the 7 station tide gauges. We used daily Mean Sea Surface (MSS) from 1995 to 2016, available on Système d'Observation du Niveau des Eaux Littorales (SONEL) networks (www.sonel.org), obtained from different tidal filters (e.g., Doodson filter and Demerliac filter) to reduce the tidal effects. Several such linear filters compute the daily mean sea levels [27,30].

### 2.3. Study Area

The study area is located along the Atlantic coast in the Bay of Biscay (42–48°N, 0–10°W), an extension of the Atlantic Ocean, off the western coast of Europe, bordered by France and Spain. In this area, the continental shelf is narrow in the south (~30 km) and extends to 180 km in the north [31]. The oceanic circulation is characterized by the presence of a large-scale gyre, the Iberian Poleward Current (IPC) [29,32] These characteristics, combined with a seasonal wind regime [30,33] and a

large amount of fresh water from river discharges [31,34], drive a complex system of coastal currents, mesoscale eddies, local upwellings, and internal tide [33,35].

In the study area, five passes of ERS-2/Envisat/SARAL were available (Figure 2a), three descending passes (#0360, #0818, #0274), and two ascending passes (#0945, #0859). Three Jason-1 and Jason-2 passes, two descending (#70, #248), and an ascending pass (#213) were available.
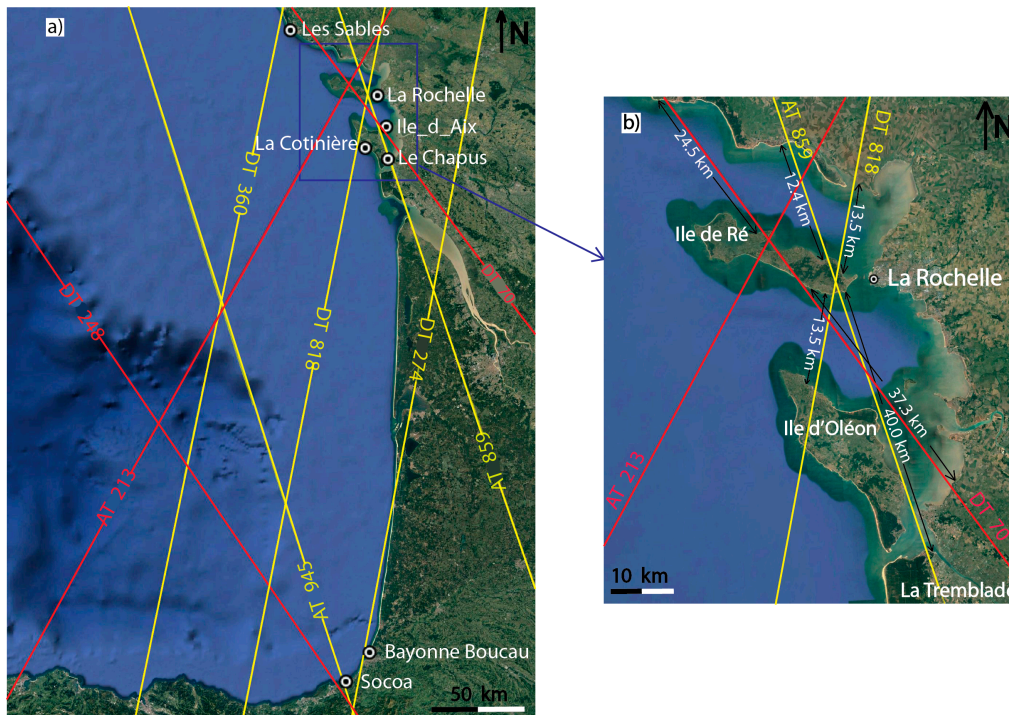


**Figure 2.** Google Earth image of the study area (**a**) with superposition of theoretical traces altimetry. Jason-1 and Jason-2 tracks are represented with red lines and ERS-2, Envisat, and SARAL tracks with yellow lines; (**b**) detail near La Rochelle tide gauge with Jason-1 and Jason-2 tracks in red lines and ERS-2, Envisat, and SARAL tracks in yellow.

Envisat and ERS-2 altimetry heights are referenced to the WGS 84 ellipsoid, and Jason-1 and 2 and SARAL are relative to the Topex/Poseidon ellipsoid. The corrections applied to the different sensors, contained in the Envisat, ERS-2, Jason-1 and 2, and SARAL GDR standard data products are listed in Table 2.

**Table 1.** Locations of the tide gauge stations and the available time period in the study area. Columns 6 and 7 show the satellite track number and the distance track–tide gauge. The green highlights the tracks close to the coastline (<15 km). The yellow tracks are located in a mixed domain between the coastal area and open ocean (15–25 km), and the red tracks the open ocean (>25 km).

| Tide Gauge Station | Longitude (°) | Latitude (°) | Validation Period | ZH/GRS80 (m) | Jason-1 and 2 | | ERS-2, Envisat, SARAL | |
|---|---|---|---|---|---|---|---|---|
| | | | | | Track | Distance (km) | Track | Distance (km) |
| Bayonne Boucau | 43.5273 | −1.5148 | 1999–2015 | 46.41 | 248 | 24.3 | 274, 945 | 3.0, 18.6 |
| Bourceranc le Chapus | 45.8534 | −1.1778 | 2012–2013 | 43.49 | 70 | 7.0 | 818, 859 | 17.8, <1 |
| Ile d'Aix | 46.0074 | −1.1743 | 2011–2015 | 43.49 | 70, 213 | 2.88, 29.0 | 818, 859 | 13.7, 4.7 |
| La Rochelle la Pallice | 46.1585 | −1.2206 | 1996–2015 | 43.46 | 70, 213 | 8.8, 16.8 | 818, 859 | 5.8, 5.4 |
| Les Sables d'Olonne | 46.4974 | −1.7935 | 1995–2015 | 44.54 | 70 | 7.0 | 360 | 6.6 |
| La Cotinière | 45.9136 | −1.3278 | 2006–2015 | 43.45 | 213 | 24.8 | 818 | 4.7 |
| Saint Jean de Luz Socoa | 43.3952 | −1.6816 | 2002–2015 | 46.64 | 248 | 5.4 | 274, 945 | 6.2, 2.1 |

**Table 2.** Ocean ranges available and corrections for each altimetry mission.

| Altimetry Mission | Period | Format | Ocean Retracking Algorithm | Corrections to the Range | | | |
|---|---|---|---|---|---|---|---|
| | | | | Ionosphere | Dry Troposphere | Wet Troposphere | Sea State Bias |
| ERS-2 | Cycle 1 (May 1995) to cycle 085 (July 2003) | REAPER GDR | MLE-3 | NIC 09 GIM | ECMWF | Radiometer ECMWF | Empirical |
| Jason-1 | Cycle 001 (January 2002) to cycle 259 (January 2009) | GDR E | MLE-3 | Bi-frequency (C-Ku) GIM model | ECMWF model derived | Jason-1 radiometer (JMR) and ECMWF model | Empirical model derived |
| Envisat | Cycle 006 (May 2002) to cycle 094 (October 2010) | GDR C v2.1 | MLE-3 | Bi-frequency (C-Ku) GIM model | ECMWF model derived | Microwave Radiometer (MWR) and ECMWF model | Empirical model derived |
| Jason-2 | Cycle 001 (July 2008) to cycle 250 (April 2015) | GDR D | MLE-4 MLE-3 | Bi-frequency (C-Ku) and GIM model | ECMWF atmospheric pressures | Jason-2 radiometer (AMR) and ECMWF model | Empirical model derived from Jason-2 data |
| SARAL | Cycle 001 (March 2013) to cycle 028 (November 2015) | GDR T | MLE-4 | GIM- derived | ECMWF model derived | Radiometer and ECMWF model | Empirical model derived |

## 3. Methods

### 3.1. SSH from Altimetry

The absolute calibration technique is required in the determination of the absolute altimeter bias. This technique requires simultaneous measurements of $SSH_{\text{in situ}}$ by an altimeter in the same terrestrial reference frame at the exact same location or comparison point. The absolute altimeter bias ($Bias_{altimeter}$) is estimated as follows [33,36]:

$$Bias_{altimeter} = SSH_{altimeter} - SSH_{\text{in situ}} - \Delta h_{geoid} \tag{1}$$

where $SSH_{altimeter}$ and $SSH_{\text{in situ}}$ are the SSH estimated from the altimeter and in situ measurements, respectively, and $\Delta h_{geoid}$ represents the difference in geoid heights between the tide gauge and the altimeter measurement locations. A negative bias indicates that the measure of the SSH by the altimeter is underestimated; either the altimeter range is being overestimated, or the orbit is biased downwards [6]. The SSH from the altimeter is given as [2,37]:

$$SSH_{altimeter} = H - \left( R + \sum \Delta R_{environmental} + \sum \Delta R_{geophysical} \right) \tag{2}$$

where $H$ is the height of the center of the mass of the satellite above the ellipsoid, estimated using the Precise Orbit Determination (POD) technique; $R$ is the nadir altimeter range from the center of the mass of the satellite to the sea surface while considering instrumental corrections; and $\sum \Delta R_{environmental}$ and $\sum \Delta R_{geophysical}$ are the sum of the environmental and geophysical corrections applied to the range, respectively. The environmental corrections are composed of the following contributions:

$$\sum \Delta R_{environmental} = \Delta R_{ion} + \Delta R_{dry} + \Delta R_{wet} + \Delta R_{SSB} \tag{3}$$

where $\Delta R_{ion}$ is the atmospheric refraction range delay due to the free electron content associated with the dielectric properties of the ionosphere, $\Delta R_{dry}$ is the atmospheric refraction range delay due to the dry gas component of the troposphere, $\Delta R_{wet}$ is the atmospheric refraction range delay due to the water vapor and the cloud liquid water content of the troposphere, and $\Delta R_{SSB}$ is the range correction caused by the various effects of the sea surface roughness within the radar footprint. This is known as sea state bias (SSB) and is the sum of electromagnetic (EM), skew, and tracker biases. The geophysical corrections are composed of the following contributions:

$$\sum \Delta R_{geophysical} = \Delta R_{load} + \Delta R_{solid\ Earth} + \Delta R_{pole} + \Delta R_{atm} \tag{4}$$

where $\Delta R_{load}$, $\Delta R_{solid\ Earth}$ $\Delta R_{pole}$, and $\Delta R_{atm}$ are the corrections accounting for crustal vertical motions due to the solid earth, pole tides, and rapid fluctuations of the atmosphere, respectively.

The leveling of the tide gauge precisely determines the ellipsoidal height ($H_0$) of the gauge zero as:

$$SSH_{\text{in situ}} = h + H_0 \tag{5}$$

where $h$ is the instantaneous stage value in the gauge record at time $t$. $H_0$ values are provided by REFMAR (Table 1).

### 3.2. SSH Processing and Editing

Altimetry SSH was obtained using the Multi-mission Altimetry Processing Software (MAPS) [35,38]. This software computes high frequency SSH referenced to the WGS84 ellipsoid along the altimeter tracks from the altimeter range and a set of corrections chosen by the user. The range can be any of the ranges available in the GDR from different retracking algorithms. MAPS allows a refined selection of the valid altimetry data to build several virtual stations where a SSH time series over the

ocean [39] or water levels over rivers and estuaries [38,40,41] can be constructed. The altimetry-based SSH were automatically computed along the track by MAPS at a 20-Hz frequency rate (i.e., ~0.35 km along the track) for Envisat, ERS-2, Jason-1, and Jason-2, and at 40 Hz (i.e., ~0.18 km along the track) for SARAL. Many different retracking algorithms are used to measure the waveforms applied to the Brown model. Range values suitable for deriving SSH were retracked using the Maximum Likelihood Estimator (MLE) retracking algorithm for all altimeters [42] The MLE3 algorithm [43] estimates with three degrees of freedom: range, significant wave height, and power, whereas the MLE4 algorithm [41,44] estimates four degrees of freedom including the three previous plus the slope of the waveform trailing edge. We used both algorithms and compared them in this study. Data processing involved three main steps: a coarse delineation of the study area using Google Earth, a refined selection of the valid altimetry data through visual inspection, and the computation of the SSH time series using all the valid points selected by the user. The average altimetry-based SSH was computed for each cycle using the median and the mean of the selected altimetry heights, along with their respective deviation, meaning their mean absolute and standard deviations, respectively.

### 3.3. Comparisons between Altimetry-Based and In Situ-Based SSH

Based on the availability of the altimetry data, the comparison with in-situ SSH, including number of cycles, bias, root means square errors (RMSE), and correlation coefficient (R), was performed using satellite data with open ocean conditions at distances between 5 km and 50 km from the coast. Depending on the frequency of sampling of each tide gauge, the maximum time-lag between in situ records and altimetry data was lower than 10 min for any measurement considered (Section 2.2).

### 3.4. Comparisons of the Atmosphere Delays over the Open Ocean

Bias and RMSE were compared between model-based and bi-frequency ionosphere corrections. Model-based and radiometer-derived wet troposphere corrections were performed over the entire Bay of Biscay. According to a prior study [42,45] the comparisons were performed in along-track cells 7 km in length (i.e., 1-Hz). More details about their definition during the complete observation period of each altimetry mission, whose data were used in this study, are available in previous reports [40,46].

## 4. Results

Comparisons between altimetry-based SSH and tide gauge records were performed at seven locations (Table 1) along the French Atlantic coast between La Rochelle and Bayonne under eight altimetry tracks (Figure 2). We will present the results for the La Rochelle tide gauge as the in situ data records exhibit a longer period of common availability with the altimetry missions than the other tide gauges, and two altimeter tracks, ascending and descending, were available for each altimetry mission. Similar results were obtained from the other tide gauges.

### 4.1. Multi-Missions Comparisons over the French Southern Part of the Bay of Biscay

The metrics compared between the altimetry-based SSH, estimated zero and five kilometers from the coast, and SSH measured by the tide gauge were: number of cycle observations (N), bias, standard deviation (SD), root mean square error (RMSE), and correlation coefficient (R) for the different SSH values. The results are outlined in Table 3 for all the tide gauges present along the French Atlantic coast of the southern part of the Bay of Biscay. The best results were obtained with SARAL (R > 0.99 and RMSE < 0.20 m) among all the tide gauges. Excellent agreement was found using Jason-1 (R > 0.9 and RMSE < 0.15 m for the majority of the time) and Jason-2 (R > 0.9 and RMSE < 0.20 m for the majority of the time). Lower but good agreement was found using Envisat (R > 0.7 for the majority of the time and RMSE < 0.21 m). For ERS-2, the quality of the SSH retrieval was variable.

**Table 3.** Comparisons of distance to the gauge, number of cycle observations (N), bias, root mean square error (RMSE), SD, and the correlation coefficient (R) from zero to five kilometers away from the coast for all tide gauge stations present along the French Atlantic coast of the southern part of the Bay of Biscay for ERS-2, Jason-1, Envisat, Jason-2, and SARAL. The ionosphere and wet troposphere corrections were derived from the Global Ionospheric Maps (GIM) and European Center for Medium Range Weather Forecasting (ECMWF) models, respectively.

| Altimeter | Station | Altimetry Track | Distance Alt/Gauge (km) | N | Bias (m) | RMSE (m) | SD (m) | R |
|---|---|---|---|---|---|---|---|---|
| | La Rochelle | 818 | 5.8 | 13 | −0.6 | 1.4 | 1.05 | 0.41 |
| ERS-2 | La Rochelle | 859 | 5.4 | 25 | −0.65 | 0.22 | 1.45 | 0.99 |
| | Bayonne Boucau | 274 | 3.0 | 21 | −1.00 | 0.89 | 1.05 | 0.51 |
| | La Rochelle | 70 | 8.8 | 97 | −0.81 | 0.29 | 0.98 | 0.93 |
| Jason-1 | La Rochelle | 213 | 16.8 | 61 | −0.73 | 0.21 | 0.71 | 0.97 |
| | Bayonne Boucau | 248 | 24.3 | 25 | −0.94 | 0.15 | 1.00 | 0.99 |
| | Saint Jean de Luz Socoa | 248 | 5.4 | 35 | −0.77 | 0.10 | 1.00 | 0.996 |
| | La Rochelle | 818 | 5.8 | 77 | 0.37 | 0.90 | 1.00 | 0.73 |
| | La Rochelle | 859 | 5.4 | 76 | 0.49 | 0.18 | 1.15 | 0.99 |
| Envisat | Bayonne Boucau | 274 | 3.0 | 42 | −0.07 | 0.77 | 0.99 | 0.67 |
| | Saint Jean de Luz Socoa | 274 | 6.2 | 51 | −0.17 | 0.63 | 0.99 | 0.8 |
| | Les Sables d'Olonne | 360 | 6.6 | 38 | 0.25 | 0.84 | 0.97 | 0.7 |
| | La Rochelle | 70 | 8.8 | 150 | −0.30 | 0.19 | 0.99 | 0.99 |
| | La Rochelle | 213 | 16.8 | 37 | −1.20 | 0.21 | 1.27 | 0.91 |
| | Bayonne Boucau | 248 | 24.3 | 118 | −0.65 | 0.34 | 1.03 | 0.93 |
| Jason-2 | Saint Jean de Luz Socoa | 248 | 5.4 | 84 | −0.78 | 0.33 | 1.03 | 0.92 |
| | Les Sables d'Olonne | 70 | 7.0 | 111 | −0.67 | 0.17 | 0.99 | 0.98 |
| | Ile d'Aix | 213 | 29.0 | 14 | −1.1 | 0.27 | 1.27 | 0.83 |
| | Ile d'Aix | 70 | 2.88 | 58 | −0.37 | 0.21 | 1.44 | 0.98 |
| | La Rochelle | 818 | 5.8 | 25 | −0.29 | 0.19 | 0.98 | 0.99 |
| | La Rochelle | 859 | 5.4 | 26 | −0.28 | 0.13 | 1.22 | 0.99 |
| | Bayonne Boucau | 274 | 3.0 | 26 | −0.83 | 0.12 | 0.94 | 0.99 |
| SARAL | Saint Jean de Luz Socoa | 274 | 6.2 | 14 | −0.80 | 0.12 | 0.94 | 0.996 |
| | Les Sables d'Olonne | 360 | 6.6 | 14 | −0.35 | 0.08 | 1.12 | 0.998 |
| | Ile d'Aix | 818 | 13.7 | 22 | −0.37 | 0.21 | 0.98 | 0.995 |
| | Ile d'Aix | 859 | 4.7 | 22 | −0.47 | 0.14 | 1.22 | 0.99 |

*4.2. Multi-Mission Comparisons at La Rochelle Tide Gauge*

The site of La Rochelle was chosen for comparisons between tide gauge records and altimetry-based SSH because the tide gauge records cover the entire observation period for the different radar altimetry missions. For all missions in this study, we considered one ascending track and one descending track. These data were compared with the La Rochelle data in terms of N, bias, SD, RMSE, and R for the different SSH values computed using all possible combinations of ocean ranges varying from zero to five kilometers to the coast (Table 4). The considerable bias between altimetry and the tide gauge five kilometers from the coast is explained, in Section 3.1, by the slope of the geoid relative to the ellipsoid. To highlight the differences between the sensors, we present the results for the SSH estimates obtained from the GIM model for the ionosphere correction and the model-based wet troposphere correction. Therefore, the complete ERS-2 record was not used; only the data acquired from 30 November 1998 (cycle 37) to 11 August 2003 (cycle 85) was used since the release of the GIM-based ionosphere correction.

The comparison results between the tide gauge records and the altimetry-based SSH from five kilometers from the coast are presented in Figure 3 for Jason-1 and Jason-2 data, and in Figure 4 for ERS-2, Envisat, and SARAL data. The quality of the results is strongly impacted by the direction of the satellite groundtrack. The results differ between the tracks where the acquisitions were performed first on the ocean and then on the land and the opposite situation. Descending track 70 passes over the Bay of Biscay for 24.5 km between the mainland and Ré Island, and then for another 37.3 km between Ré Island and the mainland, whereas ascending track 213 passes from the ocean to Ré Island and then for 12.4 km from Ré Island to the mainland (Figure 2b). For the Jason-2 data, the number of valid cycles is higher along the descending track, with 60% of 250, cycles than along the ascending track with only 15%. Therefore, even though the descending track 70 passes from land to ocean, the results obtained for this track, the RMSE of 0.19 m and R of 0.99, are better than those of the ascending track with a RMSE of 0.21 m and a R of 0.91

(Figure 3a,b). For the Jason-1 data, the number of valid cycles is higher along the descending track, with 37% of 259 cycles, than along the ascending track with only 24% valid. Accurate results were obtained for the ascending track with a RMSE of 0.21 m and a R of 0.97, which are better than those of the descending track, with a RMSE of 0.29 m and a R value of 0.93. Both were statistically representative with more than 50 samples or cycles (Figure 3c,d). The differences between the satellites (Figure 3) could account for the disparity in tracking mode between the closed-loop Poseidon-2 tracker onboard Jason-1 and the open loop (DIODE/digital elevation model) Poseidon-3 tracker mode onboard Jason-2 [44,47].

The impact of the retracking algorithm was also analyzed. The results of the comparisons between the tide gauge records and the Jason-2 track 213 altimetry-based SSH at La Rochelle, with the two available ocean retracking algorithms (MLE-4 and MLE-3), are presented in Figure S1 for distances varying from 0 to 50 km from the coast. The results show that within the zero to five kilometer zone, only 15% of cycles are valid. Furthermore, the SSH derived from altimetry over five kilometers from the coast is affected not only by less reliable geophysical and environmental corrections, but it is also influenced by the land. The RMSE and R obtained were 0.33 m and 0.8, respectively, using MLE-3, and 0.21 m and 0.91, respectively, using MLE-4.

Figure 4 shows the comparison results for ERS-2, Envisat, and SARAL virtual stations at La Rochelle. Large differences were observed between ascending track 859 and descending track 818 for all missions. As seen in Figure 1b, descending track 818 passes over the Bay of Biscay for 13.5 km between the mainland and Ré Island, and then for another 13.5 km between Ré Island and Oléron Island. Ascending track 859 passes over the Bay of Biscay for 40 km from la Tremblade over the mainland to Ré Island. For ERS-2 data, more valid cycles were found along the ascending track with 51% of 49 cycles, compared to the descending track with only 27% (Figure 4a,b). These results indicate that many cycles are affected by tracking loss effects. Much better results were obtained for the ascending track, with a RMSE of 0.22 m and a R of 0.99, than for the descending track with a RMSE of 1.4 m and a R of 0.41. This poor result can be accounted for by the low cycle number (N = 13), which is not statistically representative.

**Table 4.** Comparisons between altimetry-based SSH and in-situ SSH in La Rochelle from zero to five kilometers away from the coast (N, bias, RMSE, SD, and R) for ascending and descending tracks of sERS-2, Jason-1, Jason-2, Envisat, and SARAL satellites, and for various ionospheric and tropospheric corrections including GIM, bi-frequency, and model-based wet troposphere.

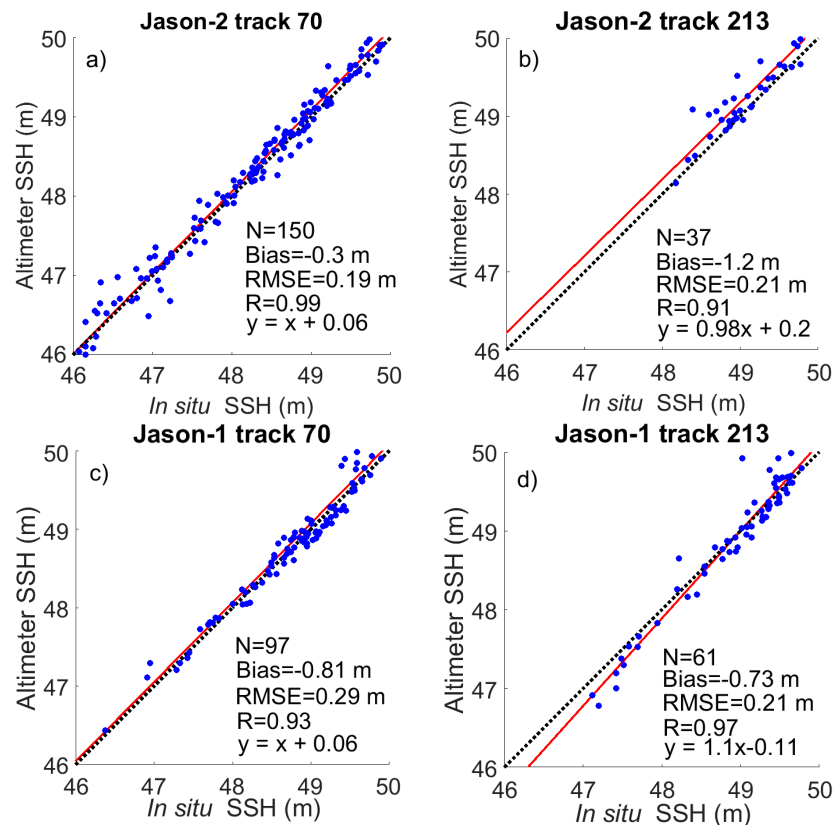| Altimeter | Correction | Descending Track | | | | | Ascending Track | | | | |
|---|---|---|---|---|---|---|---|---|---|---|---|
| | Iono-Wet Tropo | N | Bias (m) | RMSE (m) | SD (m) | R | N | Bias (m) | RMSE (m) | SD (m) | R |
| ERS-2 | Nic09-Rad | 9 | 0.32 | 1.3 | 1.12 | 0.54 | 33 | −0.40 | 0.21 | 1.41 | 0.99 |
| | GIM-Rad | 8 | 0.25 | 1.3 | 1.08 | 0.52 | 25 | −0.42 | 0.24 | 1.43 | 0.99 |
| | Nic09-Mod | 14 | −0.53 | 1.4 | 1.11 | 0.42 | 37 | −0.68 | 0.22 | 1.40 | 0.99 |
| | GIM-Mod | 13 | −0.6 | 1.4 | 1.05 | 0.41 | 25 | −0.65 | 0.22 | 1.45 | 0.99 |
| Jason-1 | Bi-Rad | 144 | −0.36 | 0.46 | 0.98 | 0.92 | 56 | −0.78 | 0.29 | 1.01 | 0.94 |
| | Bi-Mod | 97 | −0.81 | 0.46 | 1.01 | 0.82 | 54 | −0.75 | 0.28 | 1.05 | 0.94 |
| | GIM-Rad | 154 | −0.28 | 0.37 | 1.00 | 0.95 | 84 | −0.73 | 0.18 | 0.70 | 0.98 |
| | GIM-Mod | 97 | −0.81 | 0.29 | 0.98 | 0.93 | 61 | −0.73 | 0.21 | 0.71 | 0.97 |
| Envisat | Bi-Rad | 77 | 0.6 | 0.9 | 1.00 | 0.73 | 76 | 0.63 | 0.19 | 1.17 | 0.99 |
| | Bi-Mod | 77 | 0.49 | 0.9 | 1.00 | 0.73 | 76 | 0.58 | 0.18 | 1.14 | 0.99 |
| | GIM-Rad | 77 | 0.59 | 0.9 | 0.99 | 0.73 | 76 | 0.63 | 0.19 | 1.19 | 0.99 |
| | GIM-Mod | 77 | 0.37 | 0.9 | 1.00 | 0.73 | 76 | 0.49 | 0.18 | 1.15 | 0.99 |
| Jason-2 (MLE-3) | Bi-Rad | 119 | −0.61 | 0.2 | 1.02 | 0.97 | 22 | −1.20 | 0.26 | 0.75 | 0.86 |
| | Bi-Mod | 119 | −0.61 | 0.2 | 1.01 | 0.97 | 22 | −1.20 | 0.26 | 0.75 | 0.85 |
| | GIM-Rad | 132 | −0.54 | 0.22 | 0.99 | 0.98 | 42 | −1.30 | 0.33 | 0.91 | 0.81 |
| | GIM-Mod | 132 | −0.54 | 0.21 | 0.99 | 0.98 | 42 | −1.30 | 0.33 | 0.91 | 0.80 |
| Jason-2 (MLE-4) | Bi-Rad | 142 | −0.31 | 0.36 | 0.99 | 0.95 | 31 | −1.20 | 0.23 | 0.90 | 0.89 |
| | Bi-Mod | 142 | −0.31 | 0.36 | 0.99 | 0.95 | 31 | −1.20 | 0.23 | 0.90 | 0.89 |
| | GIM-Rad | 150 | −0.30 | 0.19 | 0.99 | 0.99 | 37 | −1.20 | 0.2 | 1.27 | 0.91 |
| | GIM-Mod | 150 | −0.30 | 0.19 | 0.99 | 0.99 | 37 | −1.20 | 0.21 | 1.27 | 0.91 |
| SARAL | GIM-Rad | 25 | −0.29 | 0.19 | 0.99 | 0.99 | 26 | −0.28 | 0.13 | 1.22 | 0.99 |
| | GIM-Mod | 25 | −0.29 | 0.19 | 0.98 | 0.99 | 26 | −0.28 | 0.13 | 1.22 | 0.99 |

**Figure 3.** Comparisons between in situ and altimeter-based sea level anomalies in La Rochelle for (**a**,**b**) Jason-2 and (**c**,**d**) Jason-1 for descending track 70 and ascending track 213. The ionosphere and wet troposphere corrections were derived from GIM and ECMWF models, respectively.

More data were acquired in the 330 MHz Ku chirp bandwidth acquisition mode (ocean mode with a 30-m window size) than in the 82.5 MHz Ku chirp bandwidth acquisition mode (ice mode with a 116-m window size) along the 818 ERS-2 descending track and the 859 ERS-2 ascending track. This could account for the low accuracy of the ERS-2 SSH measurement and the considerable loss of data. The number of valid cycles obtained for Envisat on the ascending and descending tracks were close to 77 cycles accounting for 82% of the total. However, the results obtained for the 859 Envisat ascending track, with a RMSE of 0.18 m and a R of 0.99, were better than those for the 818 Envisat descending track, with a RMSE of 0.9 m and a R of 0.73 (Figure 4c,d). Along the 859 Envisat ascending track, the data were acquired in the 320 MHz Ku chirp bandwidth acquisition mode with a 64-m window size. Along the 818 Envisat descending track, the data were acquired in both the 320 and 80 MHz Ku chirp bandwidth acquisition modes with 64- and 256-m window sizes, respectively, over land, and in the 320 MHz bandwidth over open ocean. Over the study area, the altimeter switched between these two modes, accounting for both the data loss and the decrease in accuracy. Similar results were found in the Gironde Estuary [38,41]. Better results were obtained using SARAL data, with a RMSE of 0.19 m and a R value of 0.99 for the 818 descending track, and a RMSE of 0.13 m and a R of 0.99 for the 859 ascending track. The number of valid cycles obtained for SARAL was 92% of the total for both the ascending and descending tracks (Figure 4e,f). This result can be accounted for by the larger effective footprint radius of ERS-2 and Envisat at Ku-band than the one of SARAL at Ka-band, and the surrounding lands along the track are encompassed in the scene observed by the altimeter. Therefore, the number of valid cycles for the SARAL altimeter are greater than the number of valid cycles with ERS-2 and Envisat. If these results are confirmed, we can attribute this accuracy to the smaller effective footprint at Ka-band. Radar echoes are less affected by the presence of land surrounding the study area.
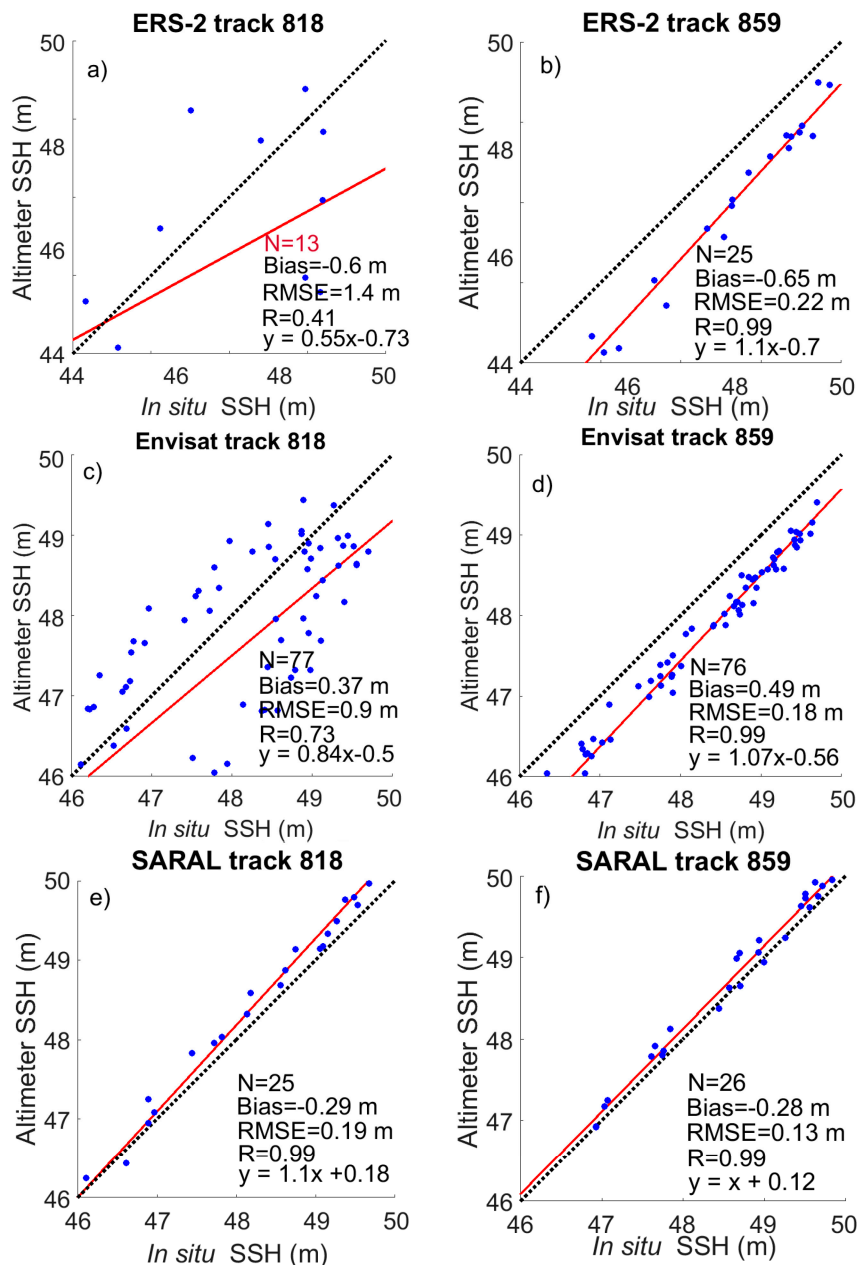
**Figure 4.** Comparisons between in situ and altimeter-based sea level anomalies in La Rochelle for (**a**,**b**) ERS-2; (**c**,**d**) Envisat; and (**e**,**f**) SARAL for descending track 0818 and ascending track 0859. The ionosphere and wet troposphere corrections were derived from GIM and ECMWF models, respectively.

*4.3. Comparisons of Atmosphere Corrections over the Open Ocean*

4.3.1. Comparisons of Bi-Frequency and Model-Based Ionospheric Corrections

The bias and RMSE for the ionosphere corrections from bi-frequency measurements and GIM model for Jason-1, Envisat, and Jason-2 using the MLE-3 and MLE-4 retracking algorithms are presented in Table 4 and Figures 5 and 6, Figures S2 and S3, respectively, over the entire southern Bay of Biscay. Low biases and RMSE, lower than 0.03 m and 0.05 m, respectively, are found when the distance to the coast is more than 25 km, except for a limited number of locations along the track where the bias reaches 0.1 to 0.2 m, and RMSE reaches up to 0.3 to 0.5 m for Envisat. The Jason-1 and Jason-2 missions exhibit very low variation differences in the ionosphere corrections along the tracks far from the shore. To reduce this variability, ionosphere corrections were smoothed on distances of several

tenths of kilometers. Conversely, a larger variability was observed along the Envisat tracks. Biases and RMSE increased when closer to the shore, reaching several tenths of centimeters. Envisat stopped operating properly at S-band in January 2008, meaning that only the GIM-based ionosphere correction was available until the end of Envisat's scientific mission in October 2010 along the nominal orbit and April 2012 on the drifting orbit.
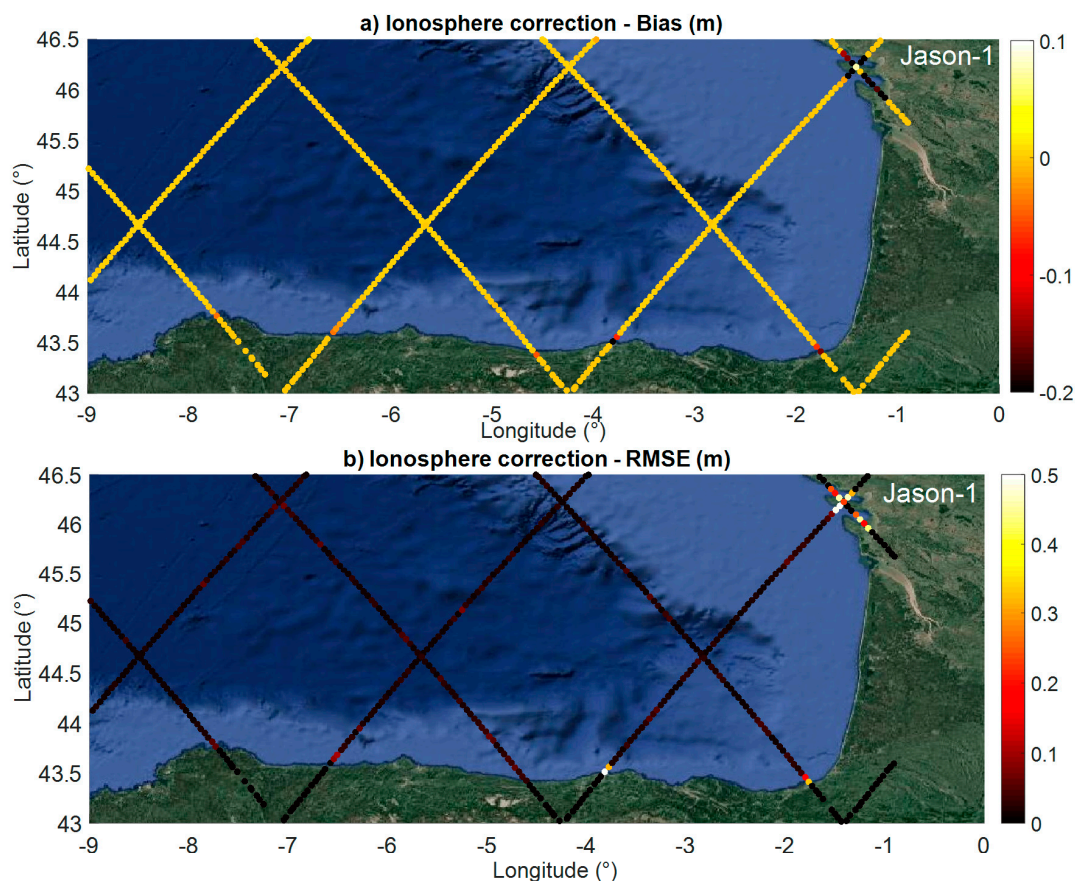


**Figure 5.** Comparison between ionosphere corrections from bi-frequency measurements and the GIM model for Jason-1: (**a**) bias and (**b**) RMSE.

Bi-frequency along-track profiles and model-based ionospheric corrections (GIM for all the missions and NIC09 for ERS-2) within 50 km of the coast are presented in Figure 7 for Jason-2 and Jason-1 (track 70), and Envisat and ERS-2 (track 859). Larger discrepancies were observed closer to the coast, reaching 0.25 m for Jason-1 when averaged over the entire observation period. Lower differences, less than 0.10 m, were observed using Jason-2 and less than 0.03 m for Envisat on average. Nevertheless, individual differences up to one meter were observed for distances from the coast, to less than 10 km between model-based and bi-frequency ionosphere corrections. Minute differences were observed between the two ionosphere correction models when compared over their common period of availability.

Due to the footprint size of the altimeter and the different frequencies used, land areas were encompassed in the image. As the radar electromagnetic wave can penetrate land surfaces with a different penetration depth, depending on the frequency and other parameters such as soil type, moisture, and roughness. For Jason-2, Jason-1 (track 213), and Envisat (track 818), within 50 km of the coast near La Rochelle, the bi-frequency-based ionospheric correction cannot be used within five kilometers of the coast, due to land contamination [45,48] (Figure 7). On the contrary, the model-based ionosphere correction presents quite stable values, in the range of a few centimeters, for the entire

observation period. For ERS-2, both GIM- and NIC09-based ionospheric corrections can be used within five kilometers of the coast (Figure 7).
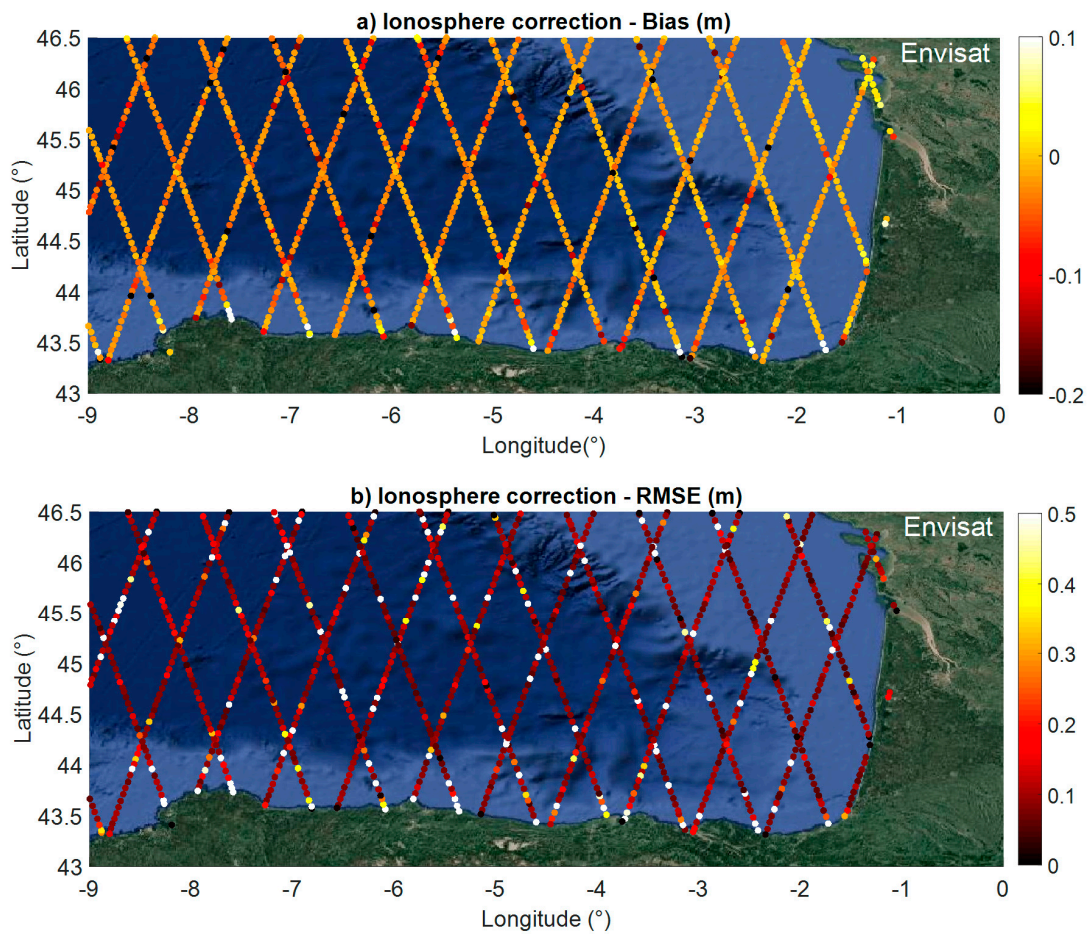


**Figure 6.** Comparison between the ionosphere corrections from bi-frequency measurements and the GIM model for Envisat: (**a**) bias and (**b**) RMSE.
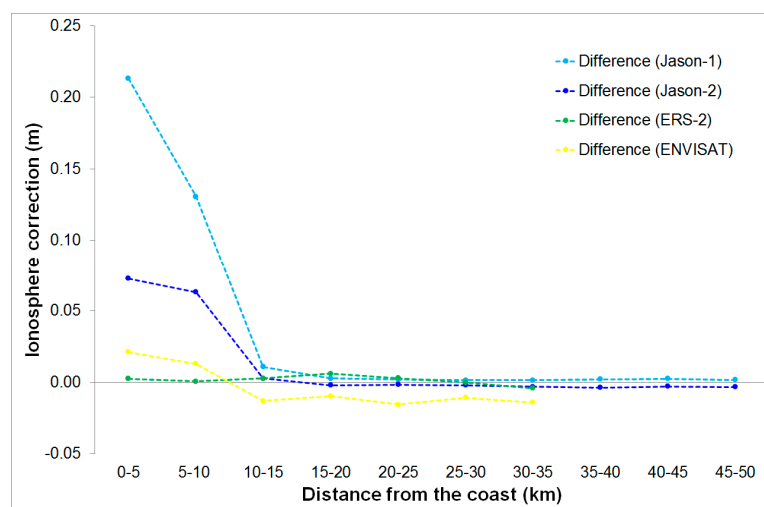


**Figure 7.** Difference between the ionosphere corrections from GIM and bi-frequency measurements for Jason-1 (light blue), Jason-2 (blue), and Envisat (yellow), and between GIM and Nic09 for ERS-2 (green) over La Rochelle within 50 km of the coast.

4.3.2. Wet Tropospheric Correction Comparison between Radiometers and ECMWF Model

Bias and RMSE for the wet troposphere corrections from radiometer measurements and the ECMWF model for Jason-1, Envisat, Jason-2, and SARAL are presented in Figures 8 and 9 and Figures S4–S6, respectively, for the entire southern Bay of Biscay. Over the open ocean, the difference between WTC derived from the ECMWF model and radiometers is negligible. Within a short distance from the coast (<25 km), both bias and RMSE increase. They remain quite small for Jason-1 (Figure 8) and Jason-2 (Figure S5) missions (lower than 0.05 m), and increase up to −0.4 m and 0.2 m for ERS-2 (Figure S4), −0.3 m and 0.2 m for Envisat (Figure 9), and −0.15 m and 0.05 m for SARAL (Figure S6), respectively.

As mentioned previously, due to the footprint size in the different frequencies used by the radiometers, land areas are encompassed in the tracks. The brightness temperatures measured in the different frequencies are affected by the presence of land in the footprint of the radiometer [11]. Corrections based on the deconvolution technique have allowed the removal of the land contribution from the signal measured by the radiometer [46,49] to provide reliable corrections up to five kilometers from the coast, as with Jason-2 (Figure S5).
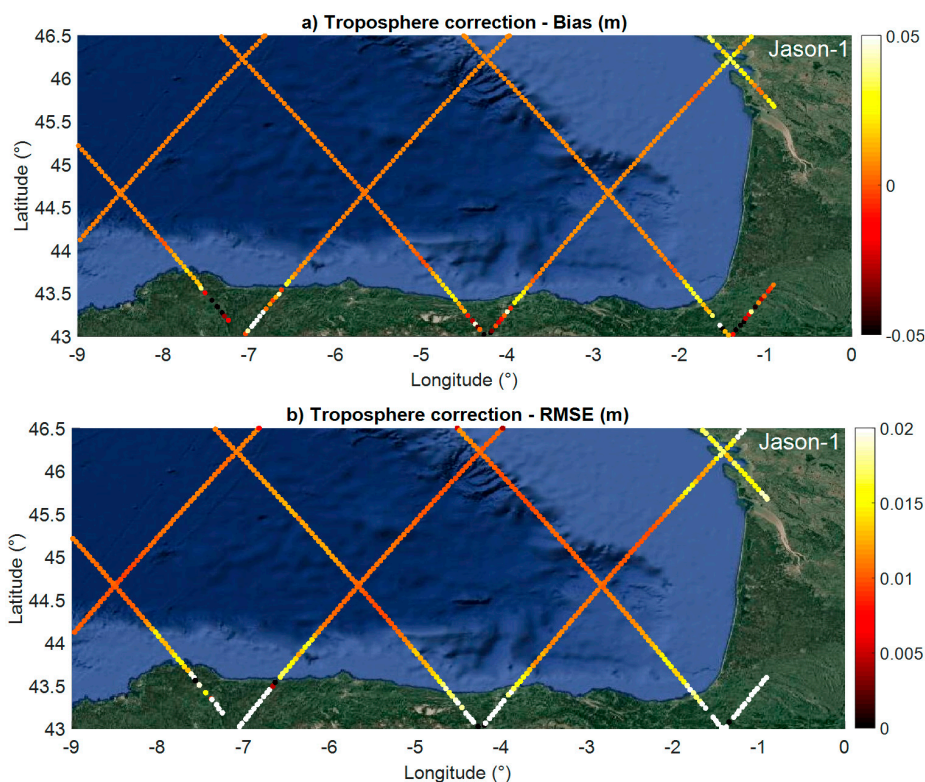


**Figure 8.** Comparison between wet troposphere corrections from radiometer measurements and the CMWF model for Jason-1b (**a**) Bias and (**b**) RMSE.

Considering the tracks of Jason-1 and Jason-2 (track 213), and ERS-2, Envisat, and SARAL (track 818) are within 50 km of the coast near La Rochelle, the improvement in the quality of the wet troposphere correction is visible (Figure 10). The wet troposphere correction derived from the ECMWF model output, considered as a reference, is quite stable against time and along the tracks. A clear improvement is observed between Jason-1, with an almost constant bias of five centimeters along the 50 km stretch, and Jason-2, with almost no bias up to 10–15 km from the coast that reaches 0.03 m at the coast, and also between ERS-2 with a small negative bias that increases from 20–25 km from the coast to reach −0.20 m at the coast, Envisat with almost no bias up to 10–15 km from the coast that reaches −0.13 m at the coast, and SARAL with almost no bias up to 10–15 km from the coast that reaches −0.06 m at the coast.
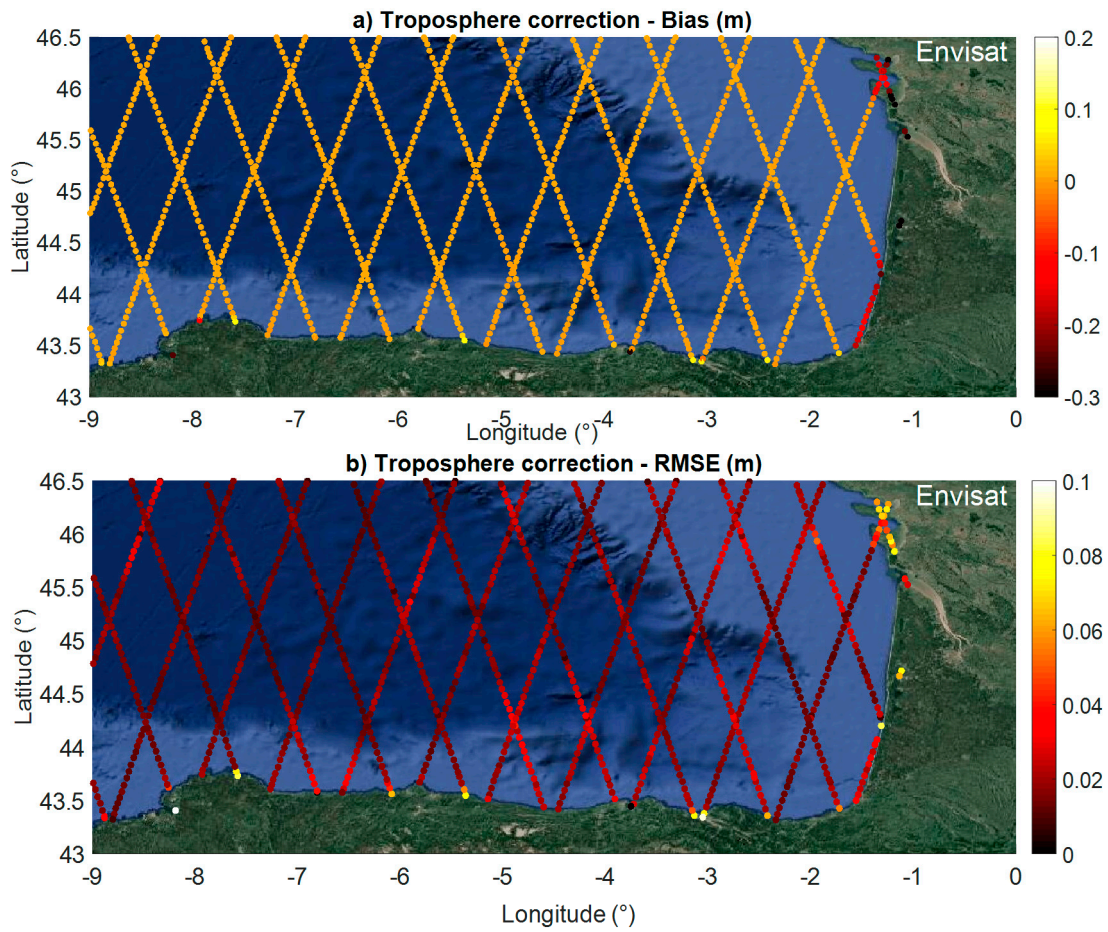
**Figure 9.** Comparison between wet troposphere corrections from radiometer measurements and the ECMWF model for Envisat: (**a**) bias and (**b**) RMSE.
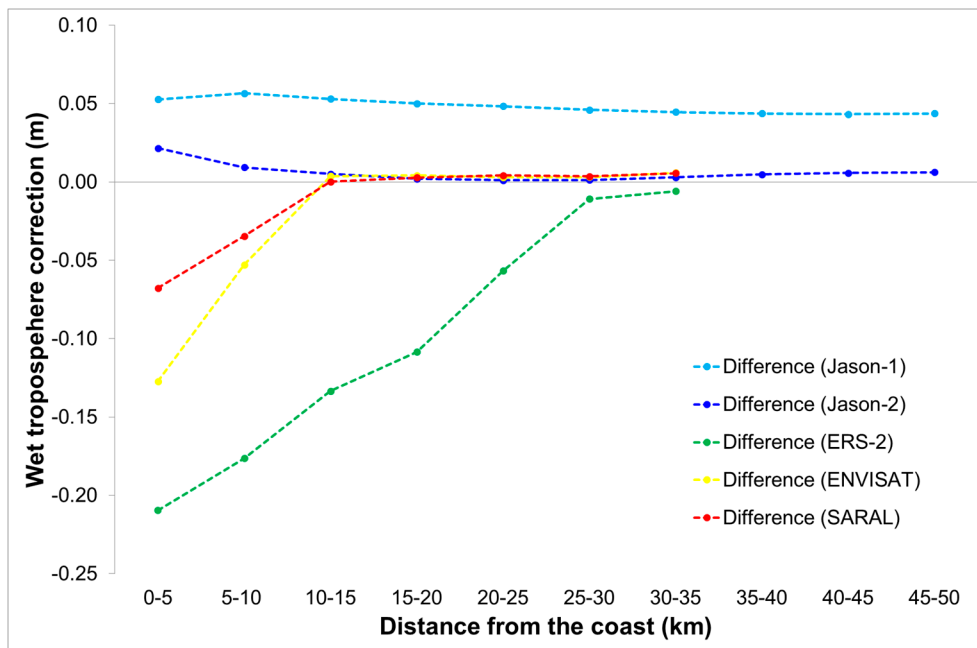


**Figure 10.** Difference between wet troposphere corrections from ECMWF and radiometer measurements for Jason-1 (light blue), Jason-2 (blue), ERS-2 (green), Envisat (yellow), and SARAL (red).

## 5. Discussion

Despite a decrease in the accuracy when approaching the coast, radar altimetry measurements can be used for monitoring the sea surface height close to the shore. The comparisons made with tide gauge records from stations located along the French Atlantic coast in the southern Bay of Biscay showed that the accuracy of the SSH estimates increased for the more recent missions on the 35-day repeating orbit from ERS-2 to SARAL, whereas similar results were observed between Jason-1 and Jason-2 on the 10-day repeating period orbit (Tables 3 and 4). Compared to ERS-2, Envisat benefits from having more acquisitions in ocean mode, at a higher bandwidth frequency mode, that allows a more accurate determination for the middle of the leading edge, and therefore for the altimeter range. SARAL, the first mission to operate at Ka-band, benefits from its smaller footprint (~8 km) [9,50] compared to all the previous altimetry missions (i.e., ~20 km for Jason-2 and ~15 km for Envisat) to obtain better estimates in terms of R (higher than 0.99), and the majority of the time, in terms of RMSE (generally lower than 0.2 m) (Table 3). In this study, if the RMSE values were large, the results presented here were obtained very close to the coast in a macro-tidal environment where the standard deviation of the SSH was generally higher than one meter (Tables 3 and 4). As seen in Figure S1, for a distance more than 10 km from the coast, the results obtained were similar to what was found at the Cal/Val sites. Better results in terms of R and RMSE were obtained when the altimeter ground-track passed from the ocean to land (e.g., track 859 of ERS-2, Envisat, and SARAL). Due to the complexity of the environment under the Jason-1 and Jason-2 tracks around the La Rochelle tide gauge, with the presence of Ré and Oléron islands, no similar conclusion was obtained. Comparisons were performed not only using classical bi-frequency-based ionosphere corrections and radiometer-derived wet troposphere corrections, as measurements were performed over open ocean, but also using corrections derived from model outputs over land, including GIM for the ionosphere and ECMWF for the wet troposphere. The analysis of these different types of corrections showed very good agreement over open ocean but more discrepancies for distances less than 25 km from the coast. However, these results were variable depending on the mission. This latter result shows that model-based ionosphere and wet troposphere corrections could be used for homogeneous long-term altimetry-based SSH from multiple missions, especially given the loss of the secondary frequency, as for Envisat. The deconvolution technique used to filter out the land contribution in the radiometer measurements enables the use of this correction up to the coast in the case of Jason-2 (Figure 10). Efforts to homogenize the corrections are needed to build long term records of altimetry-based SSH. In the near future, the Pertuis Charentais region, encompassed in a few tenths of kilometers by four tide gauge stations (La Rochelle, l'Ile d'Aix, La Cotinière, and Le Chapus) could be the first Cal/Val site located along the Atlantic coast. This group of stations benefit from numerous ascending and descending tracks from all the high-precision altimetry missions including Cryosat-2, Sentinel-3A, and the future Sentinel-3B. These stations also have a large diversity in their sea state due to their configuration in the open ocean, away from Ré and Oléron islands and the coastal part between these islands and the shore.

## 6. Conclusions

This study provides a thorough assessment of the performance of radar altimetry-based SSH for all the missions in orbit from ERS-2 to SARAL with the exception of Geosat Follow-On. From all the retracking algorithms, MLE-4 provided the most accurate estimates, especially for distances less than 10 km from the coast. The most recent missions, whose data were considered in this study, showed a clear improvement in the quality of the altimetry-derived SSH data. Results of the comparisons between in situ and Jason-2-based SSH within five kilometers of the coast had a good RMSE, lower than 0.34 m. As the descending track of ERS-2 and Envisat passes from land to ocean, the RMSE obtained was higher compared to the same in situ tide gauges, 1.4 m and 0.9 m, respectively. Due to the large footprint size of Envisat and ERS-2 (18 km), land areas were encompassed, thereby reducing accuracy. The best RMSE was less than 0.21 m for the SSH derived from the SARAL altimeter and the in situ tide gauge at the same nine locations. The comparison statistics showed that the SARAL altimeter

provides better results than other missions over the coastal area. This is due to both improvements in the processing algorithms (MLE-4 vs. MLE-3) and the use of the Ka-band for AltiKa onboard SARAL that is characterized by a smaller footprint that enables obtaining valid range estimates closer to the shore than when using the classical Ku-band.

This study showed that model-based corrections of the ionosphere (GIM) and wet troposphere (ECMWF) delays provide more realistic estimates close to the shore than the bi-frequency-based ionosphere and radiometer-based wet troposphere corrections that are generally used. Besides, these model-based corrections provide very similar values as the instrumental corrections over the open ocean, demonstrating their potential for building homogenous long term datasets.

Better estimates of SSH are likely to be provided by Jason-3, launched 17 January 2016, which can operate in open-loop mode, taking into account a priori ranges from a digital elevation model (DEM) and Sentinel-3, launched 16 February 2016. Sentinel-3 is the first altimeter with a high-resolution mode, also known as Synthetic Aperture Radar mode (SAR), on a repetitive orbit and that can also operate in open-loop. This can increase the number of independent measurements over coastal areas, ice sheet margins, land, and inland waters. The new-era coastal altimetry satellites are becoming an important part of coastal ocean observing systems [47,51].

**Author Contributions:** All of the authors of the present work contributed to the discussion of the results, as well as the writing of the manuscript. Phuong Lan Vu and Frédéric Frappart designed the study. Phuong Lan Vu, Frédéric Frappart and José Darrozes analyzed and discussed the preliminary results. Frédéric Frappart, Vincent Marieu and Fabien Blarel provided the altimetry from Multi—satellite dataset and MAPS software.

## References

1.　Fu, L.L.; Cazenave, A. *Satellite Altimetry and Earth Sciences: A Handbook of Techniques and Applications*; International Geophysics Series; Academic Press: San Diego, CA, USA, 2001; Volume 69, 463p.

2.　Frappart, F.; Blumstein, D.; Cazenave, A.; Ramillien, G.; Birol, F.; Morrow, R.; Rémy, F. Satellite Altimetry: Principles and Applications in Earth Sciences. In *Wiley Encyclopedia of Electrical and Electronics Engineering*; Webster, J., Ed.; John Wiley & Sons: Hoboken, NJ, USA, 2017; pp. 1–25.

3.　Deng, X.; Featherstone, W.E.; Hwang, C.; Berry, P.A.M. Estimation of contamination of ERS-2 and POSEIDON satellite radar altimetry close to the coasts of Australia. *Mar. Geodesy* **2002**, *25*, 249–271. [CrossRef]

4.　Deng, X.; Featherstone, W.E. A coastal retracking system for satellite radar altimeter waveforms: Application to ERS-2 around Australia. *J. Geophys. Res.* **2006**, *111*. [CrossRef]

5.　Gommenginger, C.; Thibaut, P.; Fenoglio-Marc, L.; Qyartly, G.; Deng, X.; Gomez-Enri, J.; Challenor, P.; Gao, Y. Retracking altimeter waveforms near the coasts: A review of retracking methods and some applications to coastal waveforms. In *Coastal Altimetry*; Vignudelli, S., Kostianoy, A., Cipollini, P., Benveniste, J., Eds.; Springer: Berlin/Heidelberg, Germany, 2011; pp. 61–101.

6.　Bonnefond, P.; Exertier, P.; Laurain, O.; Thibaut, P.; Mercier, F. GPS-based sea level measurements to help the characterization of land contamination in coastal areas. *Adv. Space Res.* **2013**, *51*, 1383–1399. [CrossRef]

7. Andersen, O.B.; Scharroo, R. Range and geophysical corrections in coastal regions: And implications for mean sea surface determination. In *Coastal Altimetry*; Vignudelli, S., Kostianoy, A., Cipollini, P., Benveniste, J., Eds.; Springer: Berlin/Heidelberg, Germany, 2011; pp. 103–146.

8. Robinson, A.R.; Brink, K.H. The Global Coastal Ocean: Multiscale Interdisciplinary Processes. In *The Sea*; Harvard University Press: Cambrige, UK, 2005; Volume 13, p. 1062.

9. Verron, J.; Sengenes, P.; Lambin, J.; Noubel, J.; Steunou, N.; Guillot, A.; Picot, N.; Coutin-Faye, S.; Gairola, R.; Raghava Murthy, D.V.A.; et al. The SARAL/AltiKa altimetry satellite mission. *Mar. Geodesy* **2015**, *38*, 2–21. [CrossRef]

10. Wingham, D.J.; Francis, C.R.; Baker, S.; Bouzinac, C.; Brockley, D.; Cullen, R.; de Chateau-Thierry, P.; Laxon, S.W.; Mallow, U.; Mavrocordatos, C.; et al. CryoSat: A mission to determine the fluctuations in Earth's land and marine ice fields. *Adv. Space Res.* **2006**, *37*, 841–871. [CrossRef]

11. Obligis, E.; Desportes, C.; Eymard, L.; Fernandes, M.J.; Lázaro, C.; Nunes, A. Tropospheric Corrections for Coastal Altimetry. In *Coastal Altimetry*; Vignudelli, S., Kostianoy, A., Cipollini, P., Benveniste, J., Eds.; Springer: Berlin/Heidelberg, Germany, 2011; pp. 147–176.

12. Passaro, M.; Cipollini, P.; Vignudelli, S.; Quartly, G.D.; Snaith, H.M. ALES: A multi-mission subwaveform retracker for coastal and open ocean altimetry. *Remote Sens. Environ.* **2014**, *145*, 173–189. [CrossRef]

13. Fernandes, M.J.; Lázaro, C.; Nunes, A.L.; Scharroo, R. Atmospheric Corrections for Altimetry Studies over Inland Water. *Remote Sens.* **2014**, *6*, 4952–4997. [CrossRef]

14. Birol, F.; Fuller, N.; Lyard, F.; Cancet, M.; Niño, F.; Delebecque, C.; Fleury, S.; Toublanc, F.; Melet, A.; Saraceno, M. Coastal applications from nadir altimetry: Example of the X-TRACK regional products. *Adv. Space Res.* **2017**, *59*, 936–953. [CrossRef]

15. Bonnefond, P.; Exertier, P.; Laurain, O.; Ménard, Y.; Orsoni, A.; Jan, G.; Jeansou, E. Absolute Calibration of Jason-1 and TOPEX/Poseidon Altimeters in Corsica. *Mar. Geodesy* **2003**, *26*, 261–284. [CrossRef]

16. Haines, B.J.; Desai, S.D.; Born, G.H. The Harvest experiment of the climate data record from TOPEX/Poseidon, Jason-1 and the ocean surface topography mission. *Mar. Geodesy* **2010**, *33*, 91–113. [CrossRef]

17. Mertikas, S.P.; Ioannides, R.T.; Tziavos, I.N.; Vergos, G.S.; Hausleitner, W.; Frantzis, X.; Tripolitsiotis, A.; Partsinevelos, P.; Andrikopoulos, D. Statistical models and latest results in the determination of the absolute bias for the radar altimeters of Jason satellites using the Gavdos facility. *Mar. Geodesy* **2010**, *33*, 114–149. [CrossRef]

18. Watson, C.S.; White, N.C.; Church, J.A.; Burgette, R.J.; Tregoning, P.; Coleman, R. Absolute calibration in Bass Strait, Australia: TOPEX, Jason-1 and OSTM/Jason-2. *Mar. Geodesy* **2011**, *34*, 242–260. [CrossRef]

19. Pingree, R.D.; Mardell, G.T.; New, A.L. Propagation of internal tides from the upper slopes of the Bay of Biscay. *Nature* **1986**, *321*, 154–158. [CrossRef]

20. New, A.L. Internal tidal mixing in the Bay of Biscay. *Deep Sea Res. Part A Oceanogr. Res. Pap.* **1988**, *35*, 691–709. [CrossRef]

21. Pairaud, I.L.; Lyard, F.; Auclair, F.; Letellier, T.; Marsaleix, P. Dynamics of the semi-diurnal and quarter-diurnal internal tides in the Bay of Biscay. Part 1: Barotropic tides. *Cont. Shelf Res.* **2008**, *28*, 1294–1315. [CrossRef]

22. Iijima, B.A.; Harris, I.L.; Ho, C.M.; Lindqwister, U.J.; Mannucci, A.J.; Pi, X.; Reyes, M.J.; Sparks, L.C.; Wilson, B.D. Automated daily process for global ionospheric total electron content maps and satellite ocean altimeter ionospheric calibration based on Global Positioning System data. *J. Atmos. Sol.-Terr. Phys.* **1999**, *61*, 1205–1218. [CrossRef]

23. Scharroo, R.; Smith, W.H.F. Global positioning system-based climatology for the total electron content in the ionosphere. *J. Geophys. Res.* **2010**, *115*. [CrossRef]

24. CTOH: Centre for Topographic Studies of the Oceans and Hydrosphere. Available online: http://ctoh.legos.obs-mip.fr (accessed on 4 December 2017).

25. United States Department of Agriculture. Available online: https://ipad.fas.usda.gov/cropexplorer/global_reservoir (accessed on 4 December 2017).

26. Carayon, G.; Steunou, N.; Courrière, J.; Thibaut, P. Poseidon-2 radar altimeter design and results of in-flight performances. *Mar. Geodesy* **2003**, *26*, 159–165. [CrossRef]

27. Desjonquères, J.-D.; Carayon, G.; Steunou, N.; Lambin, J. Poseidon-3 Radar Altimeter: New Modes and In-Flight Performances. *Mar. Geodesy* **2010**, *33*, 53–79. [CrossRef]

28. Zelli, C. ENVISAT RA-2 advanced radar altimeter: Instrument design and prelaunch performance assessment review. *Acta Astronaut.* **1999**, *44*, 323–333. [CrossRef]

29. Service Hydrographique et Océanographique de la Marine. Available online: http://data.shom.fr/donnes/refmar (accessed on 4 December 2017).

30. Besser, G. *Marées*; Service Hydrographique et Océanographique de la Marine: Paris, France, 1985.

31. Charria, G.; Lazure, P.; le Cann, B.; Serpette, A.; Reverdin, G.; Louazel, S.; Batifoulier, F.; Dumas, F.; Pichon, A.; Morele, Y. Surface layer circulation derived from Lagrangian drifters in the Bay of Biscay. *J. Mar. Syst.* **2013**, *109*, 60–76. [CrossRef]

32. Frouin, R.; Fiúza, A.F.G.; Ambar, I.; Boyd, T.J. Observations of a Poleward Surface Current off the Coasts of Portugal and Spain During Winter. *J. Geophys. Res.* **1990**, *95*, 679–691. [CrossRef]

33. Le Cann, B.; Pingree, R.D. Structure, strength, and seasonality of the slope current in the Bay of Biscay region. *J. Mar. Biol. Assoc.* **1990**, *70*, 857–885.

34. Lazune, P.; Jegou, A.-M.; Kerdreux, M. Analysis of salinity measurements near islands on the French continental shelf of the Bay of Biscay. *Sci. Mar.* **2006**, *70*, 7–14.

35. Pichon, A.; Correard, S. Internal tides modelling in the Bay of Biscay. Comparisons with observations. *Sci. Mar.* **2006**, *70*, 65–88. [CrossRef]

36. Ménard, Y.; Jeansou, E.; Vincent, P. Calibration of the TOPEX/POSEIDON Altimeters Additional Results at Harvest. *J. Geophys. Res.* **1994**, *99*, 24487–24504. [CrossRef]

37. Chelton, D.B.; Ries, J.C.; Haines, B.J.; Fu, L.-L.; Callahan, P.S. Satellite Altimetry. In *Satellite Altimetry and Earth Sciences*; Fu, L.-L., Cazenave, A., Eds.; Academic Press: San Diego, CA, USA, 2001; pp. 1–131.

38. Frappart, F.; Papa, F.; Marieu, V.; Malbéteau, Y.; Jordy, F.; Calmant, S.; Durand, F.; Bala, S. Preliminary assessment of SARAL/AltiKa observations over the Ganges-Brahmaputra and Irrawaddy Rivers. *Mar. Geodesy* **2015**, *38*, 568–580. [CrossRef]

39. Frappart, F.; Roussel, N.; Biancale, R.; Martinez Benjamin, J.J.; Mercier, F.; Pérosanz, F.; Garate Pasquin, J.; Martin Davila, J.; Perez Gomez, B.; Gracia Gomez, C.; et al. The 2013 Ibiza calibration campaign of Jason-2 and SARAL altimeters. *Mar. Geodesy* **2015**, *38*, 219–232. [CrossRef]

40. Frappart, F.; Legrésy, B.; Niño, F.; Blarel, F.; Fuller, N.; Fleury, S.; Birol, F.; Calmant, S. An ERS-2 altimetry reprocessing compatible with ENVISAT for long-term land and ice sheets studies. *Remote Sens. Environ.* **2016**, *184*, 558–581. [CrossRef]

41. Biancamaria, S.; Frappart, F.; Leleu, A.S.; Marieu, V.; Blumstein, D.; Boy, F.; Sottolichio, A.; Valle-Levinson, A. Satellite radar altimetry water elevations performance over a hundred meter wide river: Evaluation over the Garonne River. *Adv. Space Res.* **2017**, *59*, 128–146. [CrossRef]

42. Amarouche, L.; Thibaut, P.; Zanife, O.Z.; Dumont, J.-P.; Vincent, P.; Steunou, N. Improving the Jason-1 ground retracking to better account for attitude effects. *Mar. Geodesy* **2004**, *27*, 171–197. [CrossRef]

43. Rodríguez, E. Altimetry for non-Gaussian oceans: Height biases and estimation of parameters. *J. Geophys. Res.* **1988**, *93*, 14107–14120. [CrossRef]

44. Brown, G. The average impulse response of a rough surface and its applications. *IEEE Trans. Antennas Propag.* **1977**, *25*, 67–74. [CrossRef]

45. Astudillo, O.; Dewitte, B.; Mallet, M.; Frappart, F.; Rutllant, J.; Ramos, M.; Bravo, L.; Goubanova, K.; Illig, S. Surface winds off Peru-Chile: Observing closer to the coast from radar altimetry. *Remote Sens. Environ.* **2017**, *191*, 179–196. [CrossRef]

46. Blarel, F.; Frappart, F.; Legrésy, B.; Blumstein, D.; Rémy, F.; Fatras, C.; Mougin, E.; Papa, F.; Prigent, C.; Niño, F.; et al. Altimetry backscattering signatures at Ku and S bands over land and ice sheets. In *Remote Sensing for Agriculture, Ecosystems, and Hydrology XVII*; Neale, C.M.U., Maltese, A., Eds.; Society of Photo-Optical Instrumentation Engineers (SPIE): Bellingham, WA, USA, 2015.

47. Martin-Puig, C.; Leuliette, E.; Lillibridge, J.; Roca, M. Evaluating the Performance of Jason-2 Open-Loop and Closed-Loop Tracker Modes. *Am. Meteorol. Soc.* **2016**. [CrossRef]

48. Vignudelli, S.; Kostianoy, A.G.; Cipollini, P.; Benveniste, J. *Coastal Altimetry*; Springer-Verlag: Berlin/Heidelberg, Germany, 2011; p. 578.

49. Brown, S. A Novel Near-Land Radiometer Wet Path-Delay Retrieval Algorithm: Application to the Jason-2/OSTM Advanced Microwave Radiometer. *Geosci. Remote Sens.* **2010**, *48*, 1986–1992. [CrossRef]

50.  Bonnefond, P.; Verron, J.; Aublanc, J.; Babu, K.N.; Bergé-Nguyen, M.; Cancet, M.; Chaudhary, A.; Crétaux, J.-F.; Frappart, F.; Haines, B.J.; et al. The Benefits of the Ka-Band as Evidenced from the SARAL/AltiKa Altimetric Mission: Quality Assessment and Unique Characteristics of AltiKa Data. *Remote Sens.* **2018**, *10*, 83. [CrossRef]

51.  Liu, Y.; Kerkering, H.; Weisberg, R.H. *Coastal Ocean Observing Systems*; Elsevier: Amsterdam, The Netherlands, 2015; p. 461. ISBN 978-0-12-802022-7.